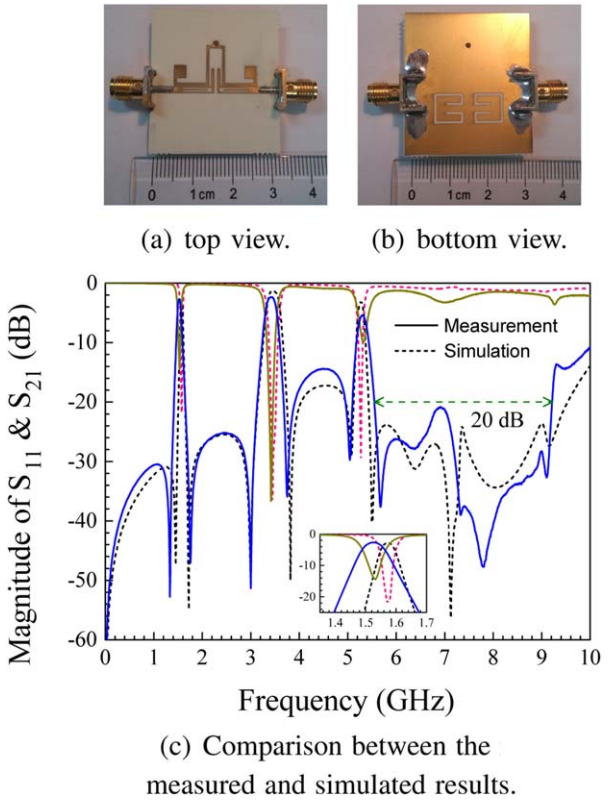

Figure 6 The proposed triband BPF. [Color figure can be viewed in the online issue, which is available at wileyonlinelibrary.com]

with the BPFs designed using the same design method in [5,6], the triband BPF here has several competitive advantages, such as greater design flexibility, higher selectivity and wider upper stopband.

3. FABRICATION AND MEASUREMENT

To verify the analyses presented above, the proposed triband BPF is fabricated. The measured and simulated results shown in Figure 6 agree well with each other, and the discrepancies are mainly due to the fabrication process and implementation. In the measurements, the three passbands are centered at 1.53, 3.42, and 5.31 GHz having 3 dB FBWs of 5.9, 5.8, and 4%, respectively. The minimal insertion losses at each passband are 2.6, 2.3, and 5.3 dB, respectively. The upper stopband rejection is better than 20 dB to more than 9.2 GHz (more than six times of the measured fundamental frequency).

4. CONCLUSION

In this letter, a novel triband BPF is proposed by incorporating two RF passages with the same feeding structure. There proved to be no cross-coupling among the two passages, and the three passbands can be designed independently with great flexibility. There are two transmission zeros beside each passband, which help to achieve high passband selectivity. At last, the feeding structure is improved by embedding two open-circuited stubs into the microstrip feed lines to eliminate the harmonic passband while the dimensions of the other structures remain the same. Compared with the filters using the same design method proposed before, the filter here exhibits several competitive advantages, such as greater design flexibility, higher selectivity and wider upper stopband.

REFERENCES

1. C.-F. Chen, T.-Y. Huang, and R.-B. Wu, Design of dual- and triple-passband filters using alternately cascaded multiband resonators, IEEE Trans Microwave Theory Tech 54 (2006), 3550–3558.
2. C.-I. Hsu, C.-H. Lee, and Y.-H. Hsieh, Tri-band bandpass filter with sharp passband skirts designed using tri-section sirs, IEEE Microwave Wireless Compon Lett 18 (2008), 19–21.
3. A. Abdel-Rahman, A. Ali, S. Amari, and A. Omar, Compact bandpass filters using defected ground structure (dgs) coupled resonators, In: 2005 IEEE MTT-S International Microwave Symposium Digest, Long Beach, CA, 2005, p. 4.
4. L. Wang and B.-R. Guan, Compact and high selectivity tri-band bpf using nested ddgsrs, Electron Lett 48 (2012), 378–379.
5. B. Wu, C.-H. Liang, P.-Y. Qin, and Q. Li, Compact dual-band filter using defected stepped impedance resonator, IEEE Microwave Wireless Compon Lett 18 (2008), 674–676.
6. X. Lai, C.-H. Liang, H. Di, and B. Wu, Design of tri-band filter based on stub loaded resonator and dgs resonator, IEEE Microwave Wireless Compon Lett 20 (2010), 265–267.
7. X.-s. Zhang, B. Liu, Y.-j. Zhao, J.-k. Wang, and W. Chen, Compact and high selectivity dual-band dual-mode microstrip bpf with five transmission zeros, Microwave Opt Technol Lett 54 (2012), 79–81.
8. C.-K. Liao, P.-L. Chi, and C.-Y. Chang, Microstrip realization of generalized chebyshev filters with box-like coupling schemes, IEEE Trans Microwave Theory Tech 55 (2007), 147–153.
9. S.W. Wong and L. Zhu, Quadruple-mode uwb bandpass filter with improved out-of-band rejection, IEEE Microwave Wireless Compon Lett 19 (2009), 152–154.
10. H. Shaman and J.-S. Hong, Ultra-wideband (uwb) bandpass filter with embedded band notch structures, IEEE Microwave Wireless Compon Lett 17 (2007), 193–195.

ANALYSIS AND DESIGN OF A BRANCH-LINE BALUN WITH HIGH-ISOLATION WIDEBAND CHARACTERISTICS

Phirun Kim, Girdhari Chaudhary, and Yongchae Jeong
Division of Electronics and Information Engineering, IT Convergence Research Center, Chonbuk National University, Jeonju, Republic of Korea; Corresponding author: ycjeong@jbnu.ac.kr

Received 3 September 2014

ABSTRACT: *This article presents a design of wideband balun with high isolation using a branch-line structure. Theoretical analysis of the proposed balun shows that the reflection coefficient characteristics with two transmission poles can be obtained by controlling the characteristic impedances of transmission lines (Z_t, Z_1, and Z_2). The high isolation can be obtained by adding a shunt coupled-line short stub and resistor (R) between the output ports. The proposed balun was designed at the center frequency (f_0) of 2.6 GHz for a current-mode class-S amplifier application. The measured results were in good agreement with the simulations, showing that power division ratios were 3.09 dB and 3.14 dB, whereas the return loss was 21.39 dB at the f_0 and higher than 20 dB over a bandwidth of 0.98 GHz (1.98–2.96 GHz). The isolation between output ports was higher than 18 dB for the bandwidth of 0.75 GHz (2.21–2.96 GHz). The measured phase difference between the output ports was 180° ± 9° over a frequency range of 2.2–2.98 GHz.* © 2015 Wiley Periodicals, Inc. Microwave Opt Technol Lett 57:1228–1234, 2015; View this article online at wileyonlinelibrary.com. DOI 10.1002/mop.29065

Key words: *branch-line balun; coupled line; isolation circuit; wideband*

1. INTRODUCTION

A balun is a three-ports circuit that is widely used in RF circuits design, such as push-pull amplifiers [1], balanced mixers [2],

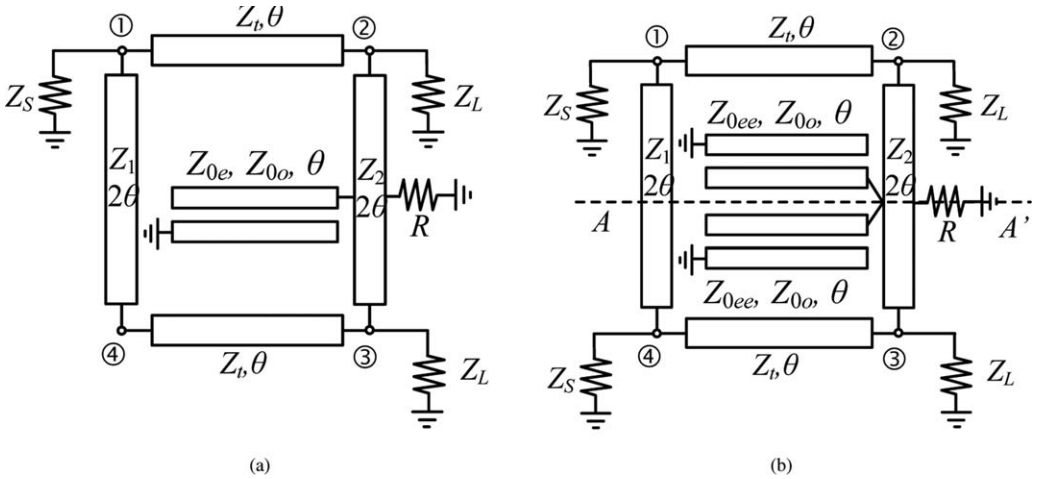

Figure 1 Structure of high-isolation wideband baluns and equivalent circuits: (a) proposed high-isolation wideband branch-line balun using a shunt-coupled line and (b) symmetrical four-ports network for even- and odd-mode analysis

and antennas [3]. In recent years, wideband baluns have been required in modern communication systems to enable high data rates and efficiency. To meet these requirements, significant efforts have been applied to designing wideband baluns using various configurations [4–17]. A three-layer wideband Marchand balun was presented in [4] using slot-coupled microstrip lines. However, this work did not consider isolation characteristics between the output ports. This is a critical design issue in the case of high-power amplifier designs, such as push-pull and current-mode class-D/S amplifiers. Moreover, the balun isolation characteristic between output ports is required to obtain a good return loss characteristics at these ports as well as to maintain RF system stability [7]. The Marchand baluns with high-isolation characteristics were introduced in [5–7] by adding resistors. However, these works were considered only at the center frequency (f_0), which can provide a narrow bandwidth characteristic. Similarly, defected ground structure coupled-line baluns were proposed in [8,9]. Although a wideband characteristic can be obtained with these structures, the isolation characteristic was not considered. In [10], a coplanar waveguide Wilkinson balun with a high-isolation characteristic was presented. However, airbridges with crossed connections are required to obtain a phase difference between output ports, which is a seemingly complicated implementation and fabrication process. Recently, three-ports baluns composed of symmetrical four-ports branch-line structures by a terminating, open/short-circuited single port were reported in [11–16]. In [12], a branch-line balun with stubs on vertical branches, which can eliminate unwanted even-mode capacitance and reduce overall circuit size, was presented. However, the circuit performances have relatively narrow bandwidths. Similarly, branch-line baluns with enhanced bandwidth were described in [13,14] by attaching a short-circuited quarter-wavelength stub to the output ports. However, these works did not consider the isolation characteristic between output ports.

In this article, a design of branch-line balun including analytical equations is presented. The proposed balun provides two transmission poles in a passband by choosing different characteristic impedances of a horizontal line (Z_t) and vertical lines (Z_1 and Z_2). By adding a resistor and a shunt-coupled line to the vertical line (Z_2), the proposed balun can match all three-ports and provide a good isolation between output ports on the wideband. For experimental verification of the proposed structure, a microstrip balun is designed, simulated, and fabricated at the f_0 of 2.6 GHz.

2. ANALYSIS

Figure 1(a) shows the structure of the proposed high-isolation wideband branch-line balun. The proposed circuit consists of a pair of horizontal quarter-wavelength ($\lambda/4$) transmission lines (TLs) with characteristic impedance Z_t and a pair of vertical half wavelength ($\lambda/2$) TLs with characteristic impedances Z_1 and Z_2. For the high isolation, a shunt coupled line and a resistor R were connected at the center of Z_2 as shown in Figure 1(a). The proposed structure is composed of symmetrical four-ports network in which one of the ports is terminated as an open-circuit. To obtain a fully symmetrical network, two parallel coupled lines are used and the open-circuited terminal is replaced by source impedance, as shown in Figure 1(b). Whereas two parallel coupled lines can be transformed into a single coupled line as shown in Figure 1(a). The even- and odd-mode excitations are applied for design equations. The equivalent circuits for even- and odd-modes are shown in Figures 2(a) and 2(b). Under the even-mode excitation, the symmetrical plane of AA' can be considered as a perfect magnetic wall (open-circuited). Therefore, the $\lambda/2$ TLs are split in half along AA' with the open circuit, as shown in Figure 2(b). The open stubs with the $\lambda/4$ TLs transform open-circuited impedance to short-circuited impedance ($Z_{\text{even}} = 0$) at the junction points ①; moreover, they can provide the transmission coefficient as zero ($T_{\text{even}} = 0$) at $f = f_0$ as the balun condition (1a). To operate the proposed circuit as the balun, another required condition [11–17] is given as (1b).

$$T_{\text{even}} = 0 \tag{1a}$$

$$Z_{\text{even}} + Z_{\text{odd}} = 2Z_{\text{s}} \tag{1b}$$

where T_{even}, Z_{even}, Z_{odd}, Z_{S}, and Z_{L} are the transmission coefficient, even- and odd-mode input impedances, source impedance, and load impedance, respectively. As shown in (1a), the balun must prevent a signal transmission during the even-mode excitation to achieve perfect amplitude and out-of-phase balances. In addition, (1b) shows that the sum of even- and odd-mode input impedances must be twice the source impedance to achieve perfect matching at the balun input port. Under the even-mode excitation, the $\lambda/2$ TLs are split in half along AA' as the open-circuited line with characteristic impedances Z_1 and Z_2, as shown in Figure 2(b). Under this excitation, (1b) reduces to (2) because of $Z_{even}=0$.

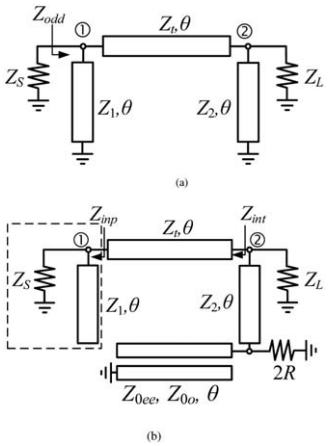

Figure 2 Equivalent circuit of proposed structure: (a) odd-mode circuit and (b) even-mode circuit

$$Z_{\text{odd}}=2Z_s \tag{2}$$

At f_0, the even-mode equivalent circuit shown in Figure 2(b) provides no signal transmission between the input and output ports due to $\lambda/4$ shunt open stubs. However, a finite level of the even-mode signal transmission exists when electrical lengths of Z_1 and Z_2 are not $\lambda/4$ in the case of $f \neq f_0$, causing amplitude and phase imbalances. In odd-mode excitation, the odd-mode equivalent circuit must transform Z_L to the required Z_{odd} to maintain a balun operation. Therefore, from Figure 2(a), the odd-mode reflection coefficient ($S_{11\text{odd}}$) and transmission coefficient ($S_{21\text{odd}}$) are given by (3).

$$S_{11\text{odd}}=\frac{A_{\text{odd}}Z_L+B_{\text{odd}}-C_{\text{odd}}rZ_L^2-D_{\text{odd}}rZ_L}{A_{\text{odd}}Z_L+B_{\text{odd}}+C_{\text{odd}}rZ_L^2+D_{\text{odd}}rZ_L} \tag{3a}$$

$$S_{21\text{odd}}=\frac{2Z_L\sqrt{r}}{A_{\text{odd}}Z_L+B_{\text{odd}}+C_{\text{odd}}rZ_L^2+D_{\text{odd}}rZ_L} \tag{3b}$$

where

$$A_{\text{odd}}=\cos\theta\left(1+\frac{Z_t}{Z_2}\right) \tag{4a}$$

$$B_{\text{odd}}=jZ_t\sin\theta \tag{4b}$$

$$C_{\text{odd}}=j\left(\frac{\sin\theta}{Z_t}-\frac{\cos\theta}{Z_2\tan\theta}-\frac{Z_t\sin\theta}{Z_1Z_2\tan^2\theta}-\frac{\cos\theta}{Z_1\tan\theta}\right) \tag{4c}$$

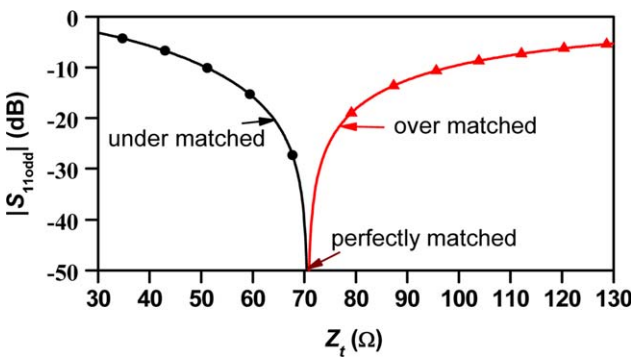

Figure 3 Input return loss characteristics at center frequency according to Z_t with $Z_L = 50\ \Omega$ and $r = 2$. [Color figure can be viewed in the online issue, which is available at wileyonlinelibrary.com]

$$D_{\text{odd}}=\cos\theta\left(1+\frac{Z_t}{Z_1}\right) \tag{4d}$$

$$r=\frac{Z_S}{Z_L} \tag{4e}$$

$$\theta=\frac{\pi f}{2f_0} \tag{4f}$$

At $f = f_0$, $S_{11\text{odd}}$ and $S_{21\text{odd}}$ of the odd-mode equivalent circuit can be reduced to (5).

$$S_{11\text{odd}}|_{f=f_0}=\frac{Z_t^2-rZ_L^2}{Z_t^2+rZ_L^2} \tag{5a}$$

$$S_{21\text{odd}}|_{f=f_0}=\pm j\frac{2Z_LZ_t\sqrt{r}}{Z_t^2+rZ_L^2} \tag{5b}$$

As shown by (5a), $S_{11\text{odd}}$ only depends on Z_t for the specified r, which is an impedance transforming ratio between Z_L and Z_S. Figure 3 shows the $S_{11\text{odd}}$ characteristic at f_0 for different values of Z_t in the case of $Z_L = Z_0 = 50\ \Omega$. From this figure, it is observed that there are three different regions [18] depending on Z_t, which can be described by (6).

$$Z_t < Z_L\sqrt{r}: \quad \text{under-matched} \tag{6a}$$

$$Z_t=Z_L\sqrt{r}: \quad \text{perfectly matched} \tag{6b}$$

$$Z_t > Z_L\sqrt{r}: \quad \text{over-matched} \tag{6c}$$

Therefore, Z_t for the specified $S_{11\text{odd}}$ is expressed in (7) for an under-matched region.

$$Z_t=Z_L\sqrt{\frac{r\left(1-S_{11\text{odd}}|_{f=f_0}\right)}{1+S_{11\text{odd}}|_{f=f_0}}} \tag{7}$$

Similarly, for an over-matched region, Z_t is found as (8).

$$Z_t=Z_L\sqrt{\frac{r\left(1+S_{11\text{odd}}|_{f=f_0}\right)}{1-S_{11\text{odd}}|_{f=f_0}}} \tag{8}$$

In a perfectly matched region, $S_{11\text{odd}}$ becomes zero, such that Z_t can be found by (9).

$$Z_t=Z_L\sqrt{r} \tag{9}$$

After finding the value of Z_t at f_0, the relation between Z_2 and Z_1 is found as (10), which can provide two poles in the passband.

$$Z_2=\frac{Z_tZ_1}{rZ_t+rZ_1-Z_1} \tag{10}$$

Figures 4(a) and 4(b) show the $S_{11\text{odd}}$ and $S_{21\text{odd}}$ characteristics of the odd-mode equivalent circuit for $S_{11\text{odd}} = -20$ dB and $S_{11\text{odd}} = -30$ dB at normalized frequency. The calculated characteristic impedances for $S_{11\text{odd}} = -20$ dB are shown in Table 1. For $S_{11\text{odd}} = -30$ dB at f_0, the characteristic impedances of TL Z_t are 72.98 Ω and 68.51 Ω for the over- and under-matched regions, respectively. In addition, the characteristic impedances of Z_2 are calculated as 21.26 Ω and 20.86 Ω for over- and under-matched regions, respectively, by choosing the

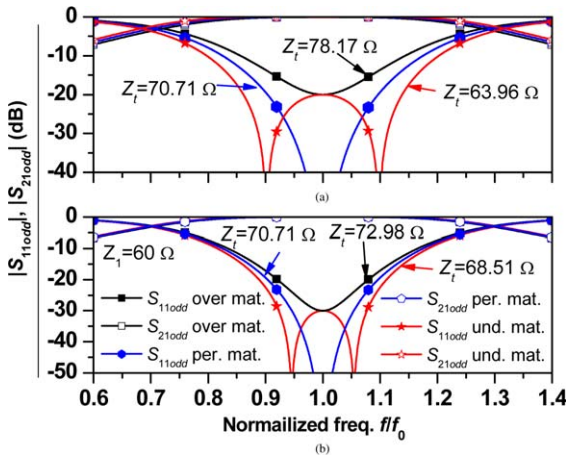

Figure 4 Reflection and transmission characteristics with different matched regions: (a) for $S_{11odd} = -20$ dB, and (b) $S_{11odd} = -30$ dB. [Color figure can be viewed in the online issue, which is available at wileyonlinelibrary.com]

same $Z_1 = 60\ \Omega$. As shown in Figures 4(a) and 4(b), two transmission poles are obtained only in the under-matched region. However, only one pole exists in the perfect and over-matched regions. Therefore, the under-matched region is preferable because two transmission poles can provide sharp and wideband return loss characteristics.

The normalized frequency locations of transmission poles in the under-matched region can be derived from (3a) which can be described by (11).

$$f_{p1,p2}/f_0 = 1 \mp \left[1 - \frac{2}{\pi}\tan^{-1}\sqrt{\frac{rZ_L^2 Z_t(Z_1+Z_t+Z_2)}{Z_1Z_2(rZ_L^2-Z_t^2)}}\right] \tag{11}$$

Using the values of Z_t and Z_2 for the under-matched region, the normalized transmission pole frequencies are calculated as $f_{p1}/f_0 = 0.902$ and $f_{p2}/f_0 = 1.098$ for $S_{11odd} = -20$ dB, and $f_{p1}/f_0 = 0.94$ and $f_{p2}/f_0 = 1.055$ for $S_{11odd} = -30$ dB.

Figure 5 presents a design graph of the under-matched region to illustrate the relation among return loss, fractional bandwidth (FBW), Z_2, and Z_t in the case of the specific $Z_1 = 60\ \Omega$. As shown in the figure, as the return loss decreases, the bandwidth of the balun increases.

Under the even-mode excitation, the symmetrical plane of AA' considered as open-circuited and resistor R is divided to half. Therefore, equivalent circuit of this mode is shown in Figiure 2(b). The output reflection coefficient (S_{22iso}) of the circuit is derived as in (12).

$$S_{22iso} = \frac{2A_{iso}R + B_{iso} - 2C_{iso}RZ_L - D_{iso}Z_L}{2A_{iso}R + B_{iso} + 2C_{iso}RZ_L + D_{iso}Z_L} \tag{12}$$

where

TABLE 1 Calculated Values of the Designed Balun with Isolation Characteristics for all Matched Regions

Z_1=60 Ω, Z_L=50 1, r=2, $Z_{0o} = Z_{0oe}$=35 Ω $S_{11\ odd} = S_{22\ iso} = -20$ dB

Mat. Con.	$Z_t(\Omega)$	$Z_2(\Omega)$	$Z_{Oe}(\Omega)$	$R(\Omega)$
Under-mat.	63.96	20.42	50.89	5.09
Over-mat.	78.17	21.68	49.52	3.84
Perf.-mat.	70.71	21.06	50.23	4.43

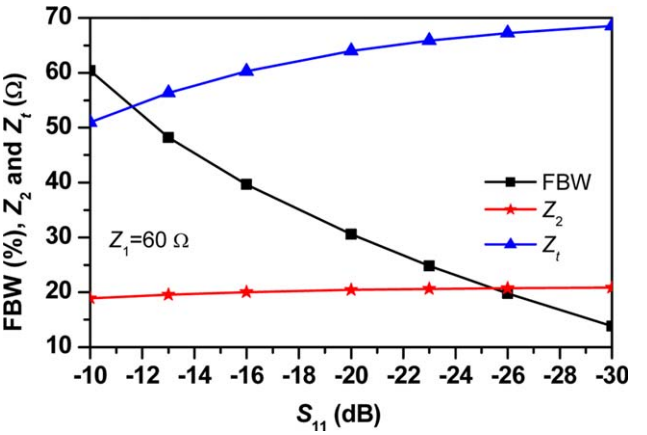

Figure 5 Relation between S_{11} and fractional bandwidth for specified value of Z_1. [Color figure can be viewed in the online issue, which is available at wileyonlinelibrary.com]

$$A_{iso} = \cos\theta\left[1 + \frac{2N_eZ_2\sin^2\theta}{(M_e^2 - N_e^2\cos^2\theta)}\right] \tag{13a}$$

$$B_{iso} = jZ_2\sin\theta \tag{13b}$$

$$C_{iso} = \frac{\cos\theta}{Z_{int}}\left(1 + \frac{2Z_2N_e\sin^2}{M_e^2 - N_e^2\cos^2\theta}\right) + j\sin\theta\left(\frac{1}{Z_2} - \frac{2N_e\cos^2\theta\sin\theta}{M_e^2 - N_e^2\cos^2\theta}\right) \tag{13c}$$

$$D_{iso} = \cos\theta + j\frac{Z_2\sin\theta}{Z_{int}} \tag{13d}$$

$$Z_{int} = Z_t\frac{Z_{inp} + jZ_t\tan\theta}{Z_t + jZ_{inp}\tan\theta} \tag{13e}$$

$$Z_{inp} = \frac{-jZ_1Z_s\cot\theta}{Z_s - jZ_1\cot\theta} \tag{13f}$$

$$M_e = Z_{0ee} - Z_{0o} \tag{13g}$$

$$N_e = Z_{0ee} + Z_{0o} \tag{13h}$$

Z_{0ee} and Z_{0o} are the even- and odd-mode impedances of even-mode equivalent circuit, respectively. At $f = f_0$, S_{22iso} of the even-mode equivalent circuit is reduced to (14).

$$S_{22iso}|_{f=f_0} = \frac{Z_2^2 - 2RZ_L}{Z_2^2 + 2RZ_L} \tag{14}$$

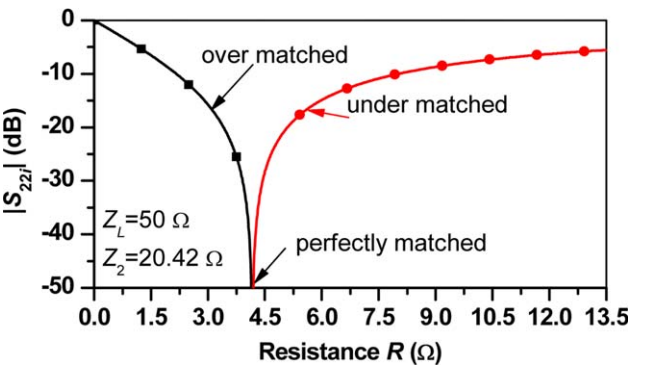

Figure 6 Output return loss characteristics at center frequency according to R. [Color figure can be viewed in the online issue, which is available at wileyonlinelibrary.com]

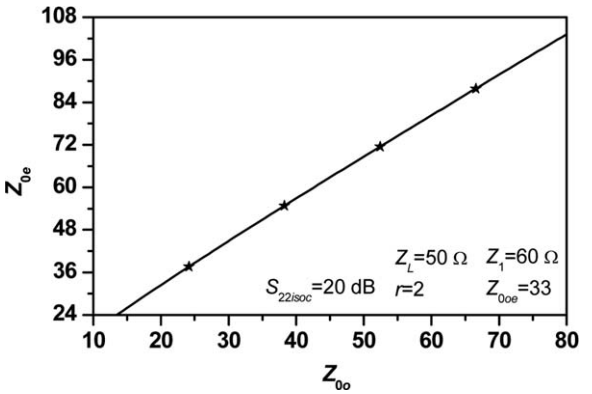

Figure 7 Relation between even- and odd-mode impedances of coupled line in Figure 1(a)

As shown by (14), $S_{22\text{iso}}$ depends on resistor R and Z_2, where Z_2 is already calculated from (10). Figure 6 shows the $S_{22\text{iso}}$ characteristics at $f = f_0$ according to R. From this figure, it shows that there are three different regions depending on R, which can be described by (15).

$$R > \frac{Z_2^2}{2Z_L} : \text{under-matched} \tag{15a}$$

$$R = \frac{Z_2^2}{2Z_L} : \text{perfectlymatched} \tag{15b}$$

$$R < \frac{Z_2^2}{2Z_L} : \text{over-matched} \tag{15c}$$

Resistance R can be defined as (16) for the under-matched region.

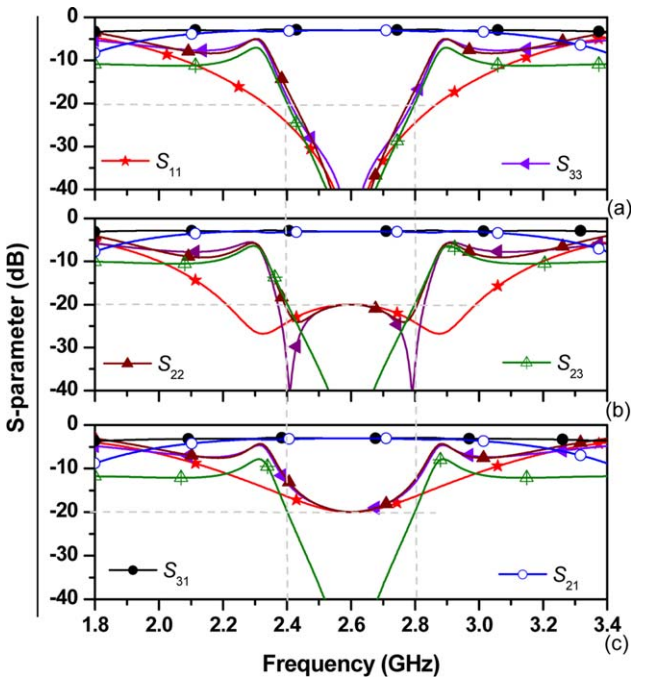

Figure 8 *S*-parameters of the high-isolation wideband balun according to different regions: (a) perfect-matched, (b) under-matched, and (c) over-matched regions. [Color figure can be viewed in the online issue, which is available at wileyonlinelibrary.com]

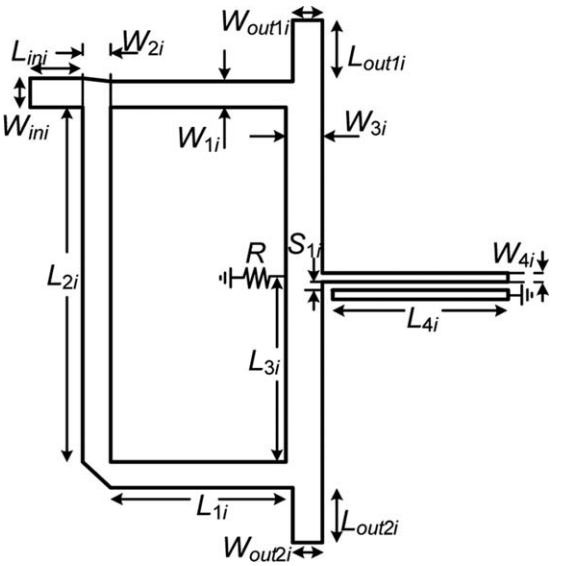

Figure 9 Layout of fabricated high-isolation wideband balun

$$R = \frac{Z_2^2\left(1+S_{22\text{iso}}|_{f=f_0}\right)}{2Z_L\left(1-S_{22\text{iso}}|_{f=f_0}\right)} \tag{16}$$

Similarly, for the over-matched region, R is defined as (17).

$$R = \frac{Z_2^2\left(1-S_{22\text{iso}}|_{f=f_0}\right)}{2Z_L\left(1+S_{22\text{iso}}|_{f=f_0}\right)} \tag{17}$$

$S_{22\text{iso}}$ becomes zero for the perfectly matched region; therefore, R is defined as (18).

$$R = \frac{Z_2^2}{2Z_L} \tag{18}$$

The input and output matched regions should be chosen as the same region to design the high-isolation wideband balun (e.g., if under-matched Z_t is chosen, then R must also be chosen as the under-matched region). After calculating R with the specified $S_{22\text{iso}}$ and the predefined Z_{0o}, the characteristic impedance of coupled line Z_{0ee} is determined to provide transmission poles of the output reflection coefficient in the passband.

From (12), the even-mode impedance of the coupled line can be found as in (19).

$$Z_{0ee} = \frac{(2Z_{0o}+x)+\sqrt{(8Z_{0o}+x)x}}{2} \tag{19}$$

where

TABLE 2 Physical Dimension of the Proposed High-Isolation Wideband Baluns Using Coupled Line

W_{1i}=58 mm	L_{1i}=21 mm
W_{2i}=1.5 mm	L_{2i}=40.8 mm
W_{3i}=3.3 mm	L_{3i}=20.75 mm
W_{4i}=0.6 mm	L_{4i}=21.5 mm
W_{2i}= $W_{\text{out1}i}$= $W_{\text{out2}i}$=2.4 mm	S_{1i}=0.28 mm
L_{ini}=$L_{\text{out1}i}$=$L_{\text{out2}i}$=5 mm	R_i=7.5 Ω

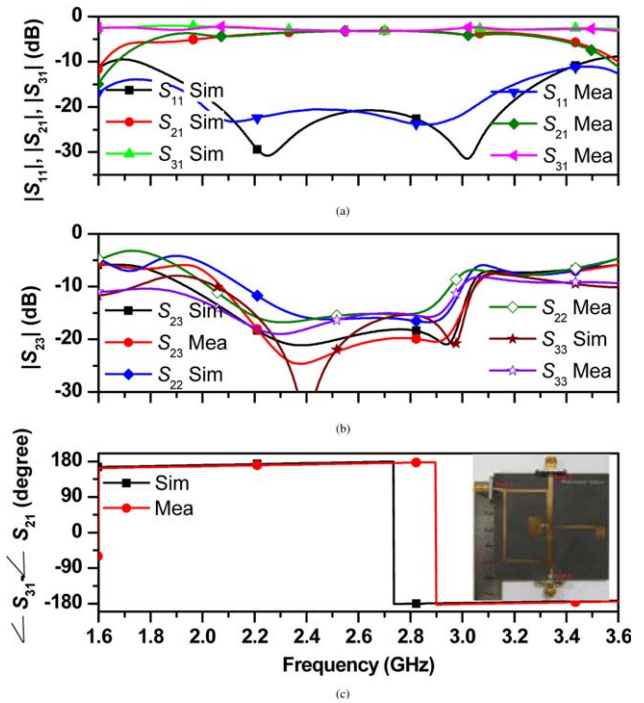

Figure 10 EM simulation and measurement of the reflection and transmission characteristics of the high-isolation balun. [Color figure can be viewed in the online issue, which is available at wileyonlinelibrary.com]

$$x = \frac{4Z_t^2 Z_2 R}{(Z_t + Z_1)Z_L Z_2 + Z_L Z_t^2 - 2RZ_t^2} \tag{20}$$

Two parallel coupled lines are transformed into a single coupled line by equating the ABCD matrix; the final circuit is shown in Figure 1(a). Z_{0e} is obtained as (21).

$$Z_{0e} = \frac{(4N_e Z_{0o} + M_e^2) + M_e\sqrt{16N_e Z_{0o} + M_e^2}}{4N_e} \tag{21}$$

where the odd-mode impedance (Z_{0o}) can be set by the designer. Figure 7 shows the relation between Z_{0e} and Z_{0o} as a design graph. As shown in the graph, the even-mode impedance increases almost linearly with Z_{0o}.

To validate the analysis, a high-isolation wideband balun was designed at f_0 = 2.6 GHz with the return loss of 20 dB. The calculated characteristic impedances and resistances of the high-isolation wideband balun using the coupled line are also shown in Table 1 according to different matched regions. Figure 8 shows the *S*-parameters of the high-isolation wideband balun for input/output perfect-, under-, and over-match regions. As shown in this figure, input and output return losses of the under-matched region demonstrate best return loss and high-isolation characteristics over the wideband.

3. SIMULATION AND MEASUREMENT RESULTS

For the experimental validation of the proposed balun, a high-isolation wideband balun using a coupled line were designed. The input and output return losses of the designed baluns were specified as 20 dB at f_0 = 2.6 GHz with terminated port impedances of 50 Ω. The circuits were fabricated on a substrate RT/Duroid 5880 of Rogers with a dielectric constant (ε_r) of 2.2 and thickness (h) of 31 mil. The electromagnetic (EM) simulation was performed using HFSS v15 from Ansoft.

The high-isolation wideband balun using a coupled line was designed for the input and output under matched regions. The calculated characteristic impedances and resistances are chosen from Table 1. Figure 9 shows the EM simulation layout of the fabricated high-isolation wideband balun using a coupled line. The overall circuit size was 60 × 60 mm^2 and the physical dimensions and component values are listed in Table 2. Figure 10 shows the EM simulation and measurement results and the photograph of the fabricated balun. The measurement results were in good agreement with the simulations. From the measurement results, the input return loss (S_{11}) was 21.39 dB at f_0 = 2.6 GHz. The bandwidth of 20 dB return loss was obtained 0.98 GHz (1.98–2.96 GHz). The magnitudes of S_{21}, S_{31}, and S_{11} measured −3.09 dB, −3.14 dB, and 21.39 dB at f_0, respectively. As shown in Figure 10(a), the amplitude division of −3 ± 0.8 dB was obtained on the bandwidth of 0.75 GHz (2.21–2.96 GHz). And the return loss better than 20 dB was obtained over the bandwidth of 0.98 GHz. Similarly, as shown in Figure 10(b), the output return losses (S_{22} and S_{33}) were −15.2 dB and −15.5 dB at f_0 and were better than −15 dB from 2.18 to 2.83 GHz, respectively. Considering that the measured results appeared acceptable, they may have been produced by some error by the parasitic of nonideal TL and fabrication tolerance of the microstrip coupled line. In addition, the measured isolation (S_{23}) of −21.84 dB was obtained at f_0, which was better than 18 dB over the bandwidth of 0.75 GHz (2.21–2.96 GHz). The measured phase difference between the two outputs was 180 ± 9° over the bandwidth of 0.78 GHz (2.2–2.98 GHz), as shown in Figure 10(c).

Table 3 compares the performance of the proposed high-isolation wideband balun using a coupled line with those in the previous example. The proposed balun is a branch-line structure implemented on microstrip PCB technology with no fabrication difficulties and which shows high-isolation and wideband characteristics.

4. CONCLUSION

In this article, a method of designing a high-isolation wideband balun using a branch-line structure was proposed. To obtain

TABLE 3 Performance Comparison of the Proposed High-Isolation Wideband Balun with Previous Studies

Reference	Center Frequency (GHz)	Fractional Bandwidth (%) Within {$\|S_{11}\|$}	Phase different (°) within {BW}	Isolation within {BW}	Structure	Size (mm^2)
[4]	2	90 {10 dB}	±1 {1.82 GHz}	n.a	slot-coupled marchand	n.a
[10]	1.5	40 {17 dB}	±10 {600 MHz}	−20 dB {=600 MHz}	CPW wilkinson	n.a
[11]	2.4	8.3 {12.5 dB}	±0.5 {200 MHz}	n.a	marchand	n.a
[12]	1	15 {20 dB}	±5 {230 MHz}	n.a	branch line	n.a
[13]	1.5	43 {15 dB}	±10 {580 MHz}	n.a	branch line	15.9×15.9
This work	2.6	**37.7** {20 **dB**}	**±9 {780 MHz}**	−18 dB {750 MHz}	branch line	60×60

high-isolation wideband characteristics, an isolation circuit using coupled lines and a resistor on the branch-line structural balun was used. Both theoretical and measurement results were provided for the validation. For experimental validations, a high-isolation wideband balun using a coupled line were designed, simulated, and fabricated. The measurement results were in good agreement with the simulation results. The proposed structure is simple to design and fabricate and is expected to be applicable to wideband RF systems.

REFERENCES

1. E. Serbryakova, A. Samulak, K. Blau, and M. Hein, Reconstruction filters for switched-mode power amplifier systems, In: Proceedings of 39th European Microwave Conference, Rome, Italy, 2009, pp. 1453–1456.
2. J. Jeong, I. Yom, and K. Yeom, An active IF balun for a double balanced resistive mixer, IEEE Microwave Wireless Compon Lett 19 (2009), 224–226.
3. P. Nguyen, A. Abbosh, and S. Crozier, Wideband and compact quasi-Yagi antenna integrated with balun of microstrip to slotline transitions, Electronics Lett 49 (2013), 88–89.
4. C. Tseng and Y. Hsiao, A new broadband marchand balun using slot-coupled microstrip lines, IEEE Micro Wireless Compon Lett 20 (2010), 157–159.
5. H. Ahn and S. Nam, New design formulas for impedance-transforming 3-dB marchand baluns, IEEE Trans Microwave Theory Techn 59 (2011), 2816–2823.
6. M. Chongcheawchamnan, C. Ng, K. Bandudej, A. Worapishet, and I. Robertson, On miniaturization isolation network of an all-ports matched impedance-transforming marchand balun, IEEE Microw Wireless Compon Lett 13 (2003), 281–283.
7. H. Ahn and T. Itoh, New isolation circuits of compact impedance-transforming 3-dB baluns for theoretically perfect isolation and matching, IEEE Trans Microwave Theory Techn 58 (2010), 3892–3902.
8. B. Li, X. Wu, J. Yang, and W. Wu, A defected-ground coupled line section with two shorts for wideband balun application, In: Proceeding of Asia Pacific Microwave Conference Singapore, 2009, pp. 2030–2032.
9. A. Abbosh, Planar ultra-wideband balun using coupled microstrip lines, Electronic Lett 49 (2013), 662–664.
10. J. Lim, D. Kim, Y. Jeong, and D. Ahn, A size-reduced CPW balun using a "X"-crossing structure, In: Proceeding of 35th European Microwave Conference Paris, France, 2005, pp. 521–524.
11. Y. Leong, K. Ang, and C. Lee, A derivation of a class of 3-port baluns from symmetrical 4-port networks, In: IEEE MTT-S International Microwave Symposium Digest Seattle, WA, 2002, pp. 1165–1168.
12. M. Park and B. Lee, Stubbed branch-line balun, IEEE Microwave Wireless Compon Lett 17 (2007), 169–171.
13. J. Li, S. Qu, and Q. Xue, Miniaturised branch-line balun with bandwidth enhancement, Electronic Lett 43 (2007), 931–932.
14. H. Zhang and H. Xin, Dual-band branch-line balun for millimeter-wave applications, In: IEEE MTT-S International Microwave Symposium Digest Boston, MA, 2009, 717–720.
15. H. Zhang, Y. Peng, and H. Xin, A tapped stepped-impedance balun with dual-band operations, IEEE Antenna Wireless Propag Lett 7 (2008), 119–122.
16. C. Shie, J. Cheng, S. Chou, and Y. Chiang, Design of a new type planar balun by using trans-directional couplers, IEEE Trans Microw Theory Techn 60 (2012), 471–476.
17. K. Ang, Y. Leong, and C. Lee, Analysis and design of miniaturized lumped-distributed impedance-transforming baluns, IEEE Trans Microwave Theory Techn 51 (2003), 1009–1017.
18. P. Kim, G. Chaudhary, and Y. Jeong, Wideband impedance transformer with out-of-band suppression characteristics, Microwave Opt Technol Lett 56 (2014), 2612–2616.

LEAKY-WAVE ANTENNA DESIGN USING QUARTER-MODE SUBSTRATE-INTEGRATED WAVEGUIDE

Dongju Lee and Sungjoon Lim
School of Electrical and Electronics Engineering, Chung-Ang University, 221 Heukseokdong, Dongjak-gu, Seoul 156-756, Republic of Korea; Corresponding author: sungjoon@cau.ac.kr

Received 1 October 2014

ABSTRACT: *A leaky-wave antenna (LWA) is designed using quarter-mode substrate-integrated waveguide (QMSIW). The LWA unit cell is miniaturized because the QMSIW size is quarter of SIW cavity. A traveling wave leaks away from open edges of the QMSIW. Its performance is verified with full-wave simulation and measurements. The main beam direction varies from 0 to 28° when frequency varies from 12.5 to 15.4 GHz.* © 2015 Wiley Periodicals, Inc. Microwave Opt Technol Lett 57:1234–1236, 2015; View this article online at wileyonlinelibrary.com. DOI 10.1002/mop.29059

Key words: *leaky-wave antenna; traveling-wave antenna; substrate-integrated waveguide; quarter-mode substrate-integrated waveguide*

1. INTRODUCTION

Waveguide structures have been widely used for millimeter-wave or high-power applications that require high performance owing to their numerous advantages, such as low-transmission loss, high-Q factor, and high-power handling capability [1]. Moreover, electromagnetic (EM) sensitivity and crosstalk can be reduced because of its enclosed structure. Nevertheless, their applications are still limited because of bulky size and difficult fabrication process.

Substrate-integrated waveguide (SIW) technology was first proposed in [2,3]. The EM properties of a waveguide can be realized using an SIW, which is manufactured using printed circuit board (PCB) process. With a waveguide, low profile and simple fabrication can be achieved while maintaining the performance.

Numerous techniques have been developed to reduce the cavity size of SIWs. Half-mode SIWs (HMSIWs), quarter-mode SIWs (QMSIWs), eighth-mode SIWs, and substrate-integrated folded waveguides have been proposed in [4–8]. These miniaturization techniques have been mostly used for small resonant antennas.

In this study, a microstrip line-fed leaky-wave antenna (LWA) is designed using SIW technology. The previously reported SIW-based LWAs used a composite right/left-handed transmission line [9] and an HMSIW [10]. However, a QMSIW has not yet been used for LWA applications. To reduce the unit cell size, a QMSIW is used, and the open sides of the QMSIW are used as leakage slots. The radiation performance of the proposed LWA is verified through full-wave analysis and experiments. Its scanning angle can be varied from 0 to 28° by varying the frequency from 12.4 to 15.4 GHz.

2. ANTENNA DESIGN

The proposed LWA is designed as a periodic structure. For periodic LWA applications, the unit cell must operate in a slow-wave mode. The unit cell is designed using a QMSIW. An ANSYS high-frequency structural simulator is used for three-dimensional full-wave EM field analysis. Figure 1 shows the geometry of the unit cell with dimensions. It is fabricated on a sheet of Rogers RT/Duroid 5880 substrate with a dielectric